Polymer 51 (2010) 3540–3550

Contents lists available at ScienceDirect

Polymer

journal homepage: www.elsevier.com/locate/polymer

The effect of carbon nanotube properties on the degree of dispersion and reinforcement of high density polyethylene

Melanie Morcom [a], Ken Atkinson [b], George P. Simon [a,*]

[a] Department of Materials Engineering, Monash University, Clayton, Victoria 3800, Australia
[b] CSIRO Materials Science and Engineering, Australia

ARTICLE INFO

Article history:
Received 21 July 2009
Received in revised form
2 March 2010
Accepted 26 April 2010
Available online 15 May 2010

Keywords:
Nanotubes
Composites
Polyethylene

ABSTRACT

The efficacy with which a range of nanotubes could reinforce a high density polyethylene (HDPE) matrix was investigated, in relation to nanotube diameter, purity, functionalization, alignment and nanotube bulk density. Composites were prepared by melt blending multiwall carbon nanotubes (MWNTs) with high density polyethylene (HDPE), followed by the injection molding of tensile specimens. At a 5 wt% loading, the most effective nanotubes were those of large diameter, received in an aligned form with low bulk density, producing a 66% increase in elastic modulus and a 69% improvement in yield stress. This was contradictory to theoretical mechanics calculations that predicted an increasing degree of reinforcement for nanotubes of reduced diameter. This difference was explained by the higher degree of dispersion observed in the composites with MWNTs of greater diameter.

1. Introduction

Theoretical and modeling studies, such as those by Thostenson and Chou [1], show that smaller diameter nanotubes have a higher potential for reinforcement due to their higher effective elastic modulus and strength. A review of the literature indicates, however, relatively few reports on the comparative reinforcing abilities of different nanotubes in the same matrix, and these have all been in non-olefinic based materials.

Gojny et al. [2] investigated the reinforcement of epoxy with various nanotubes, comparing single walled carbon nanotubes (SWNTs), double walled carbon nanotubes (DWNTs) and MWNTs, as well as amino-functionalized DWNTs and MWNTs. At the concentration of 0.1 wt%, SWNTs provided the largest increase in tensile strength and DWNTs the greatest improvement in elastic modulus. At higher concentrations (up to 0.5 wt%), amino-functionalized DWNTs showed the largest increase in both elastic modulus and strength. Since the reinforcing potential of SWNTs is higher due to their higher values of strength and elastic modulus, it is likely that the poorer properties of the SWNT–epoxy composites at concentrations greater than 0.1 wt% were due to a lack of dispersion. Likewise, the amino-functionalization of the DWNTs was thought to bring about a higher degree of dispersion at the higher concentrations (and thus an increase in elastic modulus) by increasing the surface polarity of the carbon nanotubes that interacted with the matrix.

Cadek et al. [3] studied the reinforcement effects of six different types of carbon nanotubes on freestanding poly(vinyl alcohol) films prepared by solution mixing at concentrations of 0.005 vol fraction (~1 wt%). The low diameter MWNTs gave the highest level of reinforcement, the level of reinforcement being inversely proportional to nanotube diameter. The polymer was found to crystallize on the surface of the nanotubes, thus leading to a greater degree of reinforcement due to the higher modulus of this induced crystalline phase. The coating was the same thickness for each type of nanotube and thus the degree of crystallinity was linearly dependent on nanotube concentration and inversely proportional to the diameter of the nanotubes. The higher reinforcement provided by the finer MWNTs in their work may thus have been due to the increased crystallinity of the composite rather than being directly due to higher stiffness and strength imparted by the nanotubes.

Potschke et al. [4] investigated the effect of MWNT diameter on both the dispersion and the mechanical properties of polycarbonate nanocomposites. By adjusting the temperature at which the MWNTs were synthesized, MWNTs with mean diameters of 22 and 28 nm were produced while maintaining lengths of up to 10 μm in both samples. Larger diameter MWNTs were found to be better dispersed in the polycarbonate by melt mixing than the thinner nanotubes, however there was no observable effect of nanotube diameter on the stress–strain curves of composites.

The work reported in this paper explores the extent to which the nanotube diameter has an effect on the effective reinforcement of

* Corresponding author. Tel.: +61 3 9905 4936; fax: +61 3 9905 4934.
E-mail address: george.simon@eng.monash.edu.au (G.P. Simon).

0032-3861/$ – see front matter © 2010 Elsevier Ltd. All rights reserved.
doi:10.1016/j.polymer.2010.04.053

MWNT–polymer composites and whether functionalization also influences such reinforcement. It was also of interest to investigate the significance of how the form in which the nanotubes were supplied influenced the resultant degree of dispersion, and the effect on the degree of nanotube reinforcement.

2. Experimental

2.1. Materials

The MWNTs were either manufactured in our laboratories (CSIRO Materials Science and Engineering) (denoted as CSIRO MWNTs), or were purchased from Nanocyl (Belgium). The CSIRO MWNTs were produced using a continuous catalyst injection process [5] with an in-house designed and built 63 mm ID quartz reactor packed with quartz glass slides. The reactor was placed in a 3-zone split tube furnace, flushed and run with argon as a carrier gas, and heated to 750 °C (full length). Separate heaters were used to maintain an injection port temperature of 120 °C and an outlet port temperature of 150 °C. A filtered solution of ferrocene (1% w/w) in Xylene was injected into the reactor at a rate of 3.5 g/h for 8 h. At the end of a run, the reactor was flushed for a further 10 min before cooling. Using this method, nanotubes were grown on the quartz substrate as a relatively densely-packed forest that was 1–3 mm in height. Only products from the central 100 mm zone of the furnace were selected for this study and will herein be referred to as CSIRO MWNTs.

Four other sets of nanotubes, also produced by catalytic carbon vapor deposition, were sourced from Nanocyl SA. These nanotubes were NC-7000 (Thin MWNTs), NC-3100 (purified, thin MWNTs), NC-3101 (COOH functionalized MWNTs), and MWNTs described as purified and very thin. In this work these nanotubes were labeled Nanocyl-T, Nanocyl-PT, Nanocyl-COOH and Nanocyl-PVT respectively.

The HDPE used in this work was produced by Quenos (HDPE390), with a molecular weight, M_w, of 58 886 and polydispersity of 5.815.

2.2. Analysis of nanotubes

The nanotubes were characterized using transmission electron microscopy (Philips TEM 420 for the CSIRO MWNTs and Philips CM20 TEM for the Nanocyl MWNTs) and scanning electron microscopy (SEM) (Philips XL-30 FESEM). For SEM analysis the nanotube powder was placed directly on SEM stubs using carbon tape, while for TEM analysis the nanotubes were first suspended in ethanol prior to deposition on the TEM grid. For each MWNT type, Leica software was used to measure the internal and external diameters of 100 MWNTs from high magnification TEM images. Lower magnification TEM images were also used to measure the lengths of 50 nanotubes for each MWNT type. These values were used to calculate the average diameter, length and aspect ratio for each nanotube type before processing.

The average density of the nanotubes, ρ_{NT} was determined by both pycnometry and TEM, using a method published by Thostenson and Chou [1] where the density of individual MWNTs is calculated by assuming that the graphitic layers of the tube have the same density as graphite ($\rho_g = 2.25$ g/cm^3):

$$\rho_{NT} = \frac{\rho_g(d^2 - d_i^2)}{d^2} \quad (1)$$

where d_i is the internal and d the external diameter of a nanotube. The specific surface area (SA) of the nanotubes was also calculated from the ratio of the surface area of the nanotubes ($2\pi rl$) to their mass ($\pi r^2 l\rho$):

$$SA = \frac{4}{d\rho} \quad (2)$$

The average effective elastic modulus of these nanotubes was calculated using the method of Thostenson and Chou [1], who assumed that a MWNT acts like a large SWNT with weak, interwall interactions, resulting in the outer layer of the MWNT carrying almost the entire load transferred at the nanotube–matrix interface. Following their procedure, the effective nanotube modulus, E_{eff}, was calculated by assuming the elastic modulus of the outer wall of the nanotube (E_{NT}) applied across the whole cross-section of the nanotube, i.e.:

$$E_{eff} = \frac{4t}{d}E_{NT} \quad (3)$$

where d is the diameter of the nanotube, t is the thickness of the outer layer ($\sim$0.34 nm [1]). The elastic modulus of the outer wall of the nanotube was taken as 1 TPa [1], which is approximately that of the in-plane modulus of graphite [6,7]. Equation (3) is only valid when $(t/d) < 0.25$.

2.3. Composite blending

MWNT–HDPE nanocomposites were prepared at a 5 wt% concentration by feeding the MWNTs and HDPE pellets into a Haake Mini-Lab twin-screw extruder (Thermo Electron Corp., Hamburg, Germany) (a conical twin-screw compounder with an integrated backflow channel), and processing for 10 min at 240 °C using co-rotating screws at 50 RPM. At the completion of mixing, the melt was extruded into the heated barrel of a DSM Injection Moulder (DSM Xplore, Geleen, The Netherlands), which used a plunger driven by compressed air to inject the melt into a tensile specimen mold held at 50 °C, the standard dog-bone specimen having a gauge length of 30 mm, width of 5 mm and thickness of 1.5 mm.

2.4. Analysis of dispersion

To assess the degree of nanotube dispersion at a micron scale, 2 μm thick sections were sliced from the moldings with a Reichert Ultracut S Microtome using a 30° diamond knife, the samples being cooled to −60 °C to enable smooth cutting. These sections were placed on a drop of paraffin oil on a glass slide, covered with a cover slip and imaged using an optical microscope. The fracture surfaces of the failed tensile specimens were also analyzed using a Philips XL-30 FESEM to investigate whether nanotube agglomerates were present. A 5 kV accelerating voltage was used, the samples being gold sputter coated to prevent charging and surface heating.

2.5. Mechanical properties

An Instron 5848 Microtester was used to conduct tensile tests of the injection molded specimens. The gauge length was 30 mm for all samples and the rate of extension was 5 mm/min to ensure compliance with ASTM D638-01. To calculate the breaking strains of nanocomposites with high ductility (300% strain was the maximum range of the Instron 5848 Microtester), additional specimens were prepared and tested on the larger Instron 5566 using the same extension rate.

3. Results

3.1. Analysis of nanotubes

SEM micrographs (Fig. 1) show that the CSIRO, Nanocyl-T and Nanocyl-PT MWNTs all grew in an aligned, forest-like form. The CSIRO MWNTs appeared to have significant spacing between the nanotubes, whereas the Nanocyl-T and Nanocyl-PT nanotubes had a more dense form with much lower inter-tube spacing. This was consistent with observations made during handling, the CSIRO MWNTs having low bulk density, taking up over twice the volume of any of the Nanocyl MWNTs (for the same weight).

The as-received Nanocyl-PVT MWNTs (Fig. 1(d)) and Nanocyl-COOH MWNTs (Fig. 1(e)) appear as dense clumps on the SEM micrographs. This form may be due to the chemical treatments undergone during purification and functionalization, the process of suspending in solution and then drying likely to result in a denser, tangled form.

TEM micrographs in Fig. 2 highlight the significantly larger diameters of the CSIRO MWNTs compared to the Nanocyl MWNTs. Fe particles are visible in the walls of these nanotubes due to the continuous flow of iron catalyst during the CVD process, however only small quantities of amorphous carbon are observed. Nanocyl-T MWNTs appeared relatively pure, with only small quantities of amorphous carbon present, however according to the data sheet for this material up to 5 wt% metal oxide is present in these MWNTs. Nanocyl-PT MWNTs are a purified version of the Nanocyl-T MWNTs, the purification process removing the metal oxide particles, with TEM showing no evidence of non-nanotube, carbonaceous material. Nanocyl-PVT MWNTs are the thinnest nanotubes studied with TEM images showing a high concentration of non-nanotube amorphous material ('cloudy' regions). Nanocyl-COOH MWNTs are, according to Nanocyl, the same as the Nanocyl-PT MWNTs except for the addition of 4% COOH functionalization. TEM analysis found these MWNTs to be relatively clean with only small quantities of amorphous carbon on the surfaces of the MWNTs.

Histograms in Fig. 3 show the range in diameters for each MWNT type (measured using TEM), while the average lengths and diameters of the nanotubes are shown in Table 1, along with the average aspect ratios, densities, surface areas and effective elastic modulus calculated from these values. It should be noted that the density measurements in this table were calculated using TEM measurements, as pycnometry was found to give inconsistent results due to adsorption of helium onto the surfaces of the nanotubes.

3.2. Analysis of dispersion

Transmission optical microscopy of cryo-microtomed sections of the HDPE390 nanocomposites was used to assess the level of dispersion of the nanotubes in the composites. The micrographs in

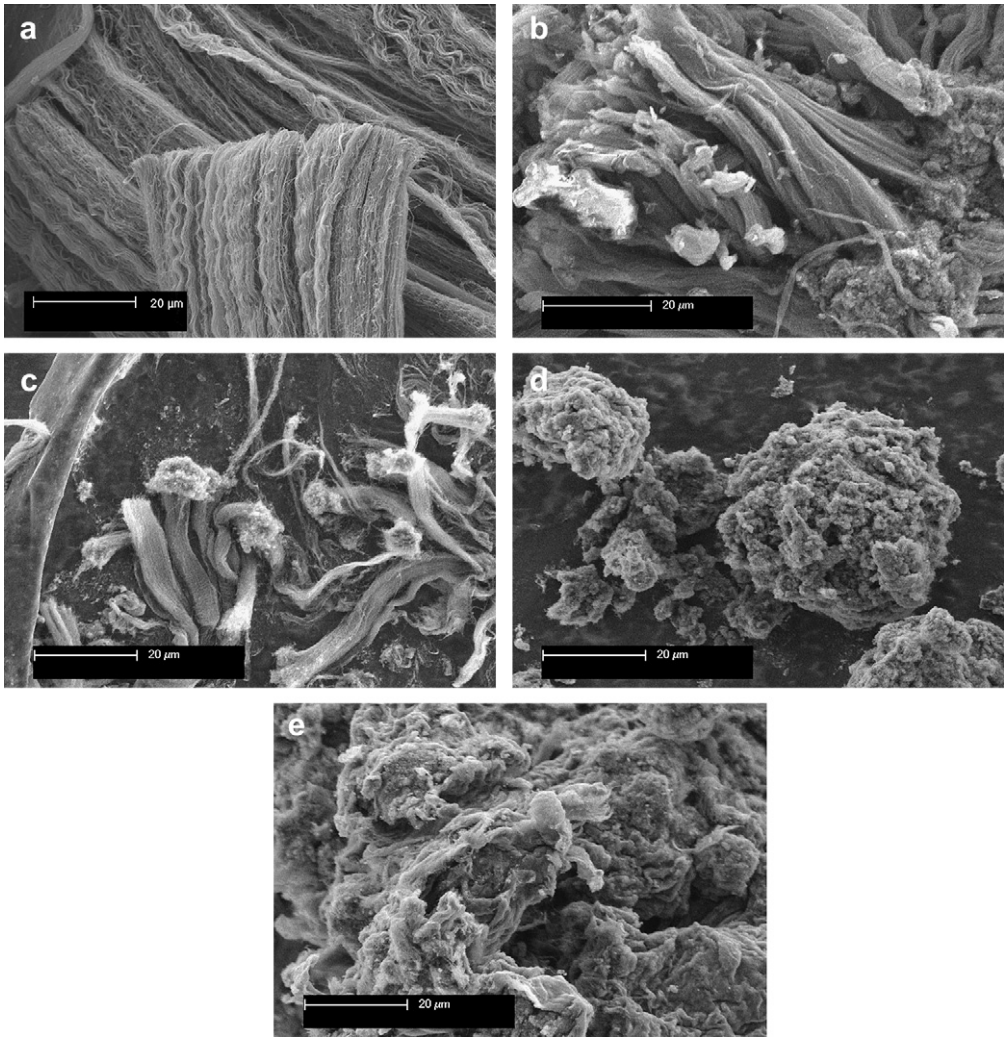

Fig. 1. SEM micrographs of the various MWNTs, illustrating the morphology in which they were received: (a) CSIRO; (b) Nanocyl-T; (c) Nanocyl-PT; (d) Nanocyl-PVT and (e) Nanocyl-COOH.

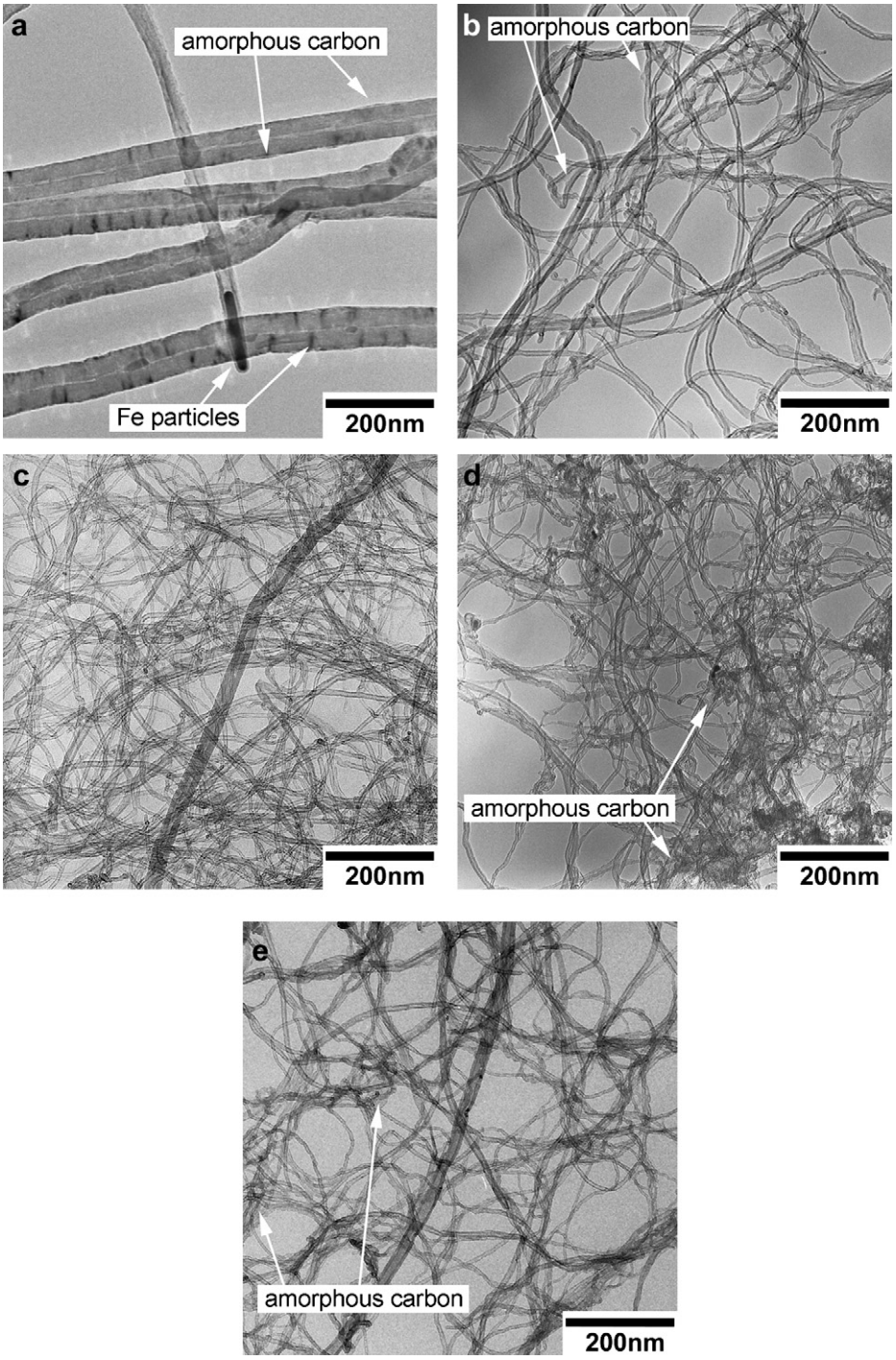

Fig. 2. TEM micrographs of the MWNTs, showing the significant variations in diameter and purity between the various MWNTs: (a) CSIRO; (b) Nanocyl-T; (c) Nanocyl-PT; (d) Nanocyl-PVT and (e) Nanocyl-COOH.

Fig. 4 show that the highest degree of dispersion was achieved for the CSIRO MWNTs, as evidenced by the presence of fewer clumps of nanotubes that were generally less than 10 μm in extent. Additionally, the edges of these clumps/agglomerates were non-distinct, suggesting a gradual transition in nanotube concentration. The overall background color, which includes the non-clumped regions, was also darker here than for the micrographs of the other composites suggesting a higher concentration of nanotubes in the non-clumped regions.

In comparison the Nanocyl-T and Nanocyl-PT composites showed low levels of nanotube dispersion, with micrographs showing a large number of clumps up to 25 μm in size. The overall background color (non-clumped regions) was not as dark as that seen for the CSIRO MWNT composites, indicating that the concentration of MWNTs in these regions was significantly lower. Micrographs of the Nanocyl-PVT composites suggested a higher level of dispersion; while there were still a large number of agglomerates with sharply defined boundaries, they were generally less than 5 μm in size, significantly smaller than those observed in the Nanocyl-T and Nanocyl-PT composites.

The composites made with the Nanocyl-COOH MWNTs showed relatively low levels of dispersion, with micrographs showing

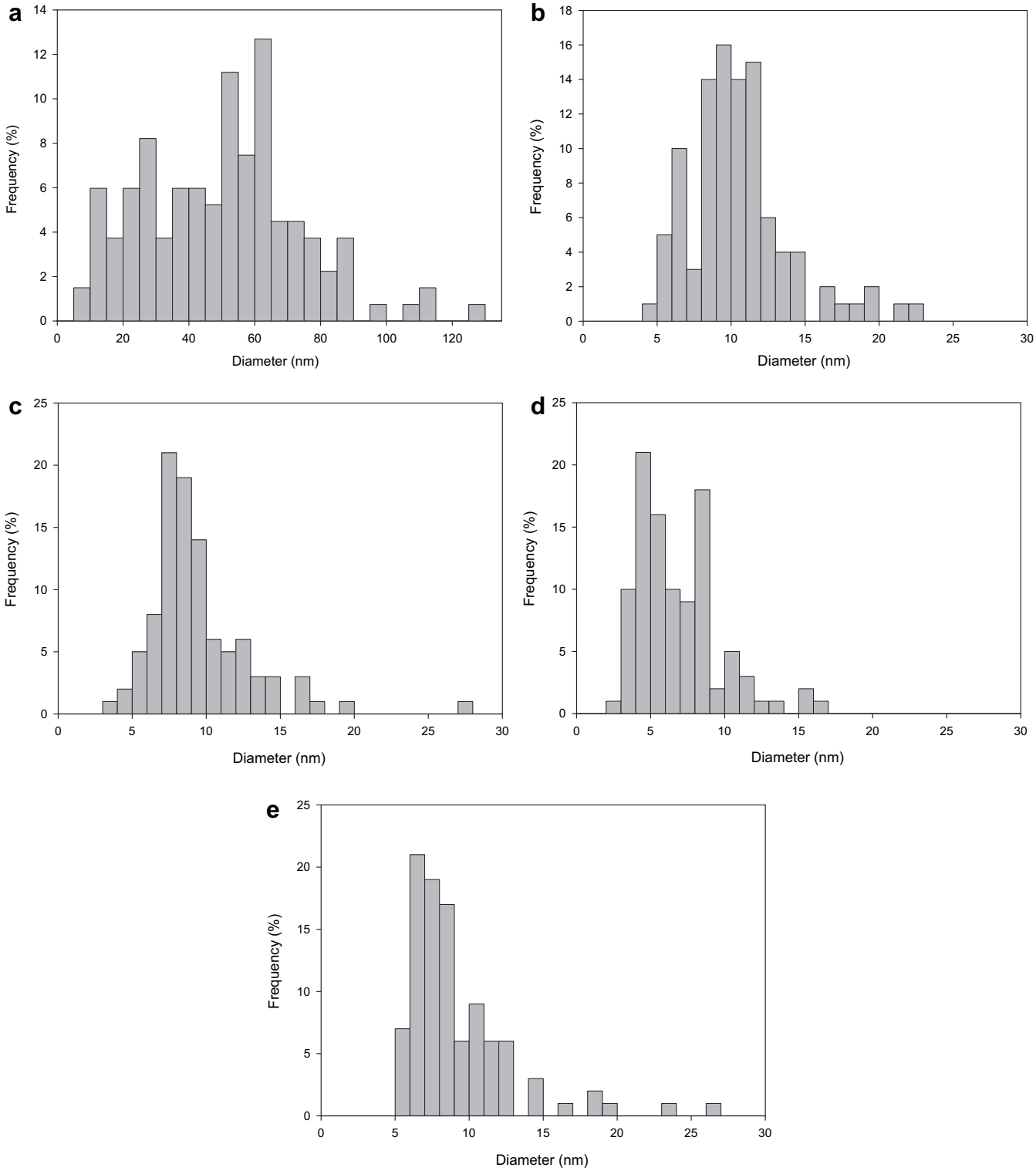

Fig. 3. Histograms showing the distribution of nanotube diameters for each nanotube type: (a) CSIRO; (b) Nanocyl-T; (c) Nanocyl-PT; (d) Nanocyl-PVT and (e) Nanocyl-COOH.

large agglomerates up to 20 μm in diameter. Away from these agglomerates there existed both transparent regions (indicating very low MWNT concentration), along with 'cloudy' regions where nanotubes had dispersed well through the polymer. This is likely in part due to the functionalized nature of these MWNTs (with −COOH groups) resulting in an increase in nanotube polarity, increasing the interaction between nanotubes and possibly inhibiting their dispersion in the non-polar HDPE.

SEM analysis of the fracture surfaces of the composites (Fig. 5) yielded similar conclusions. While the particular polymer matrix used in this work made this technique difficult (due to the high levels of localized plastic deformation at the point of failure),

Table 1
Properties of the as-received MWNTs as measured using TEM and SEM.

	CSIRO	Nanocyl-T	Nanocyl-PT	Nanocyl-PVT	Nanocyl-COOH
Length (μm)	15 ± 2	0.7 ± 0.1	1.7 ± 0.2	0.8 ± 0.1	1.2 ± 0.1
Diameter (nm)	50 ± 2	10.4 ± 0.3	9.5 ± 0.3	6.8 ± 0.3	9.2 ± 0.4
Aspect ratio	300 ± 50	70 ± 10	180 ± 30	120 ± 20	130 ± 20
Density (g/cm^3)	2.06 ± 0.03	1.85 ± 0.02	1.80 ± 0.02	1.62 ± 0.04	1.75 ± 0.02
Surface area (m^2/g)	56 ± 5	115 ± 4	105 ± 5	150 ± 9	115 ± 5
E_{eff} (GPa)	21.8 ± 1.5	200 ± 10	190 ± 10	250 ± 50	200 ± 10
Aligned	yes	yes	yes	no	no

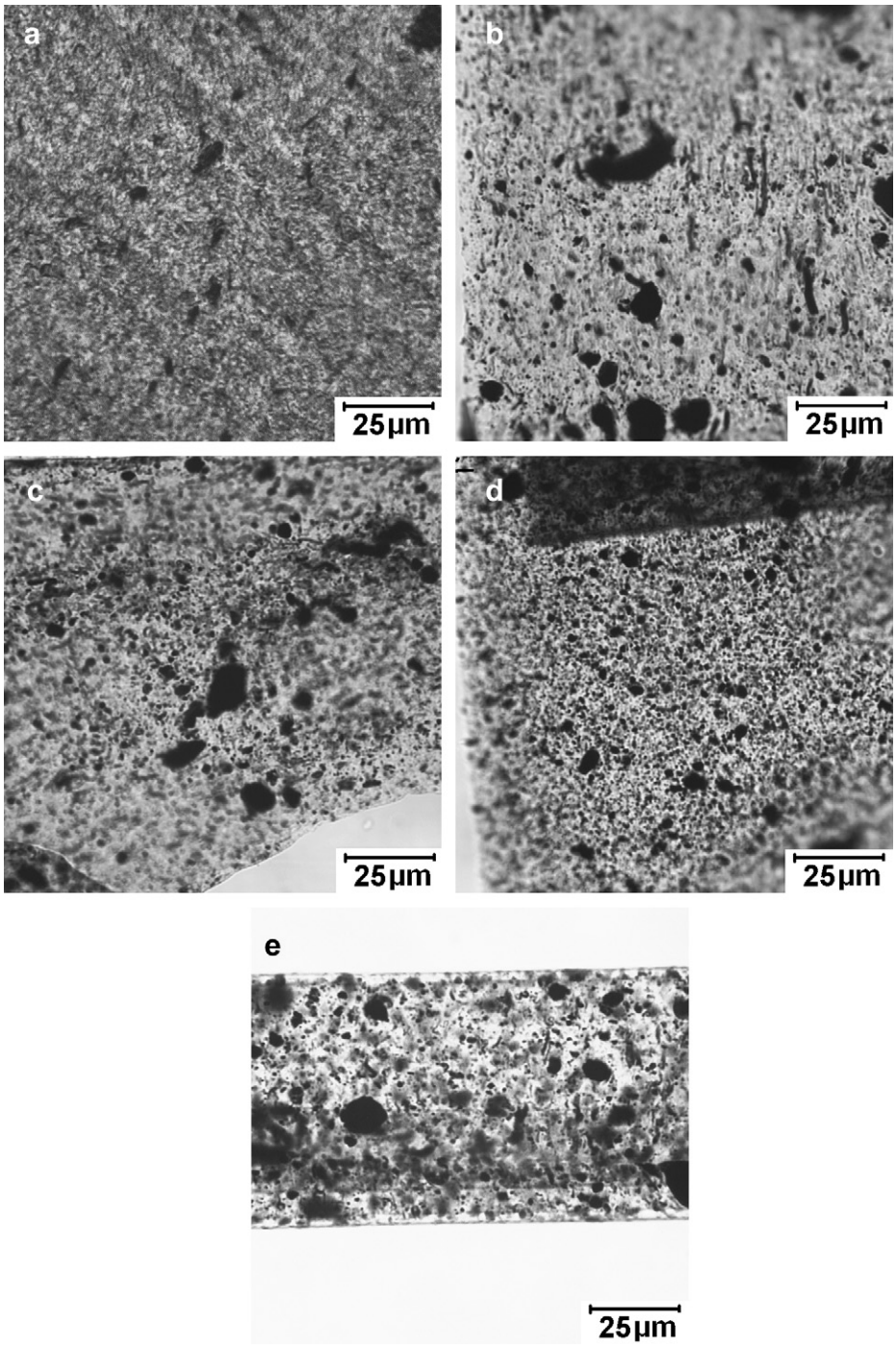

Fig. 4. Optical micrographs indicating differences in the level of the dispersion of the various MWNTs in HDPE at a 5 wt% concentration: (a) CSIRO; (b) Nanocyl-T; (c) Nanocyl-PT; (d) Nanocyl-PVT and (e) Nanocyl-COOH.

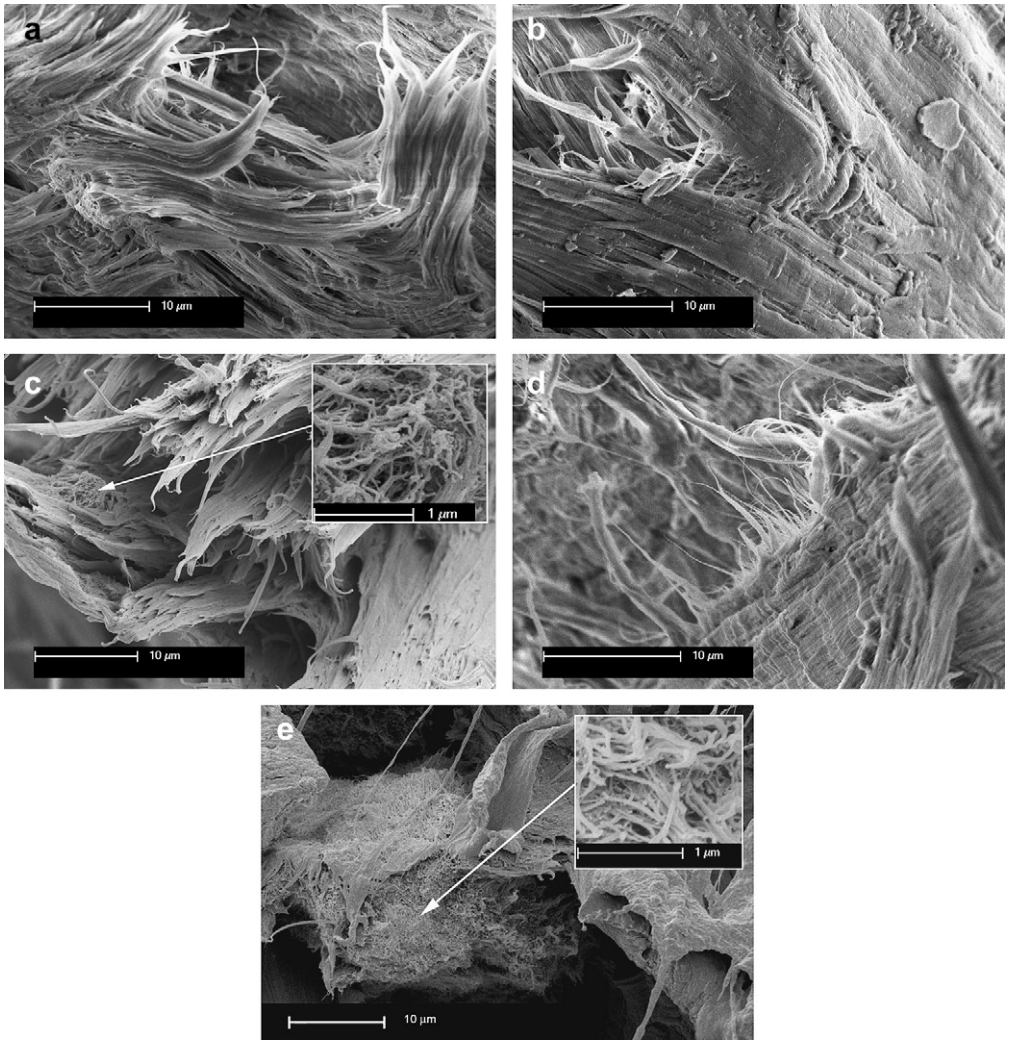

Fig. 5. Fracture surfaces of MWNT–HDPE nanocomposites: (a) CSIRO; (b) Nanocyl-T; (c) Nanocyl-PT; (d) Nanocyl-PVT and (e) Nanocyl-COOH.

examination of the fracture surfaces only found evidence of nanotube agglomerates on the Nanocyl-PT composites and Nanocyl-COOH composites. Fig. 5(c) shows an agglomerate approximately 6 μm in size in a Nanocyl-PT MWNT composite while Fig. 5(e) shows a larger clump greater than 20 μm in breadth in a Nanocyl-COOH composite.

3.3. Mechanical properties of the nanocomposites

At the 5 wt% loading used in this work, the addition of MWNTs resulted in an increase in elastic modulus for all the nanocomposites (Fig. 6). The CSIRO MWNTs produced the greatest effect, an increase of 66 ± 6%, followed by the Nanocyl-PT MWNTs, which produced a 29 ± 4% increase. The functionalization process used to produce the Nanocyl-COOH MWNTs resulted in these MWNTs being less effective (than the Nanocyl-PT MWNTs), while the high concentration of impurities is likely to have been a major cause of the Nanocyl-T and Nanocyl-PVT MWNTs providing an even smaller effect.

Composite theory states that the elastic modulus of a nanocomposite is dependent on the effective elastic modulus and aspect ratios of the fibers, together with the degree of fiber alignment. In addition, the purity of the fibers and degree of dispersion also play parts, with effective reinforcement requiring that individual nanotubes are coated with polymer to ensure load transfer from matrix to nanotube. The Halpin–Tsai Equation [8] for randomly aligned composites has been used to predict the elastic modulus of a composite, E_c

$$\frac{E_c}{E_m} = \frac{3}{8}\left(\frac{1+\zeta\eta_L V_f}{1-\eta_L V_f}\right) + \frac{5}{8}\left(\frac{1+2\eta_T V_f}{1-\eta_T V_f}\right) \tag{4}$$

$$\text{where } \zeta = 2l/D,\ \eta_L = \frac{(E_f/E_m)-1}{(E_f/E_m)+\zeta},\ \text{and } \eta_T = \frac{(E_f/E_m)-1}{(E_f/E_m)+2}$$

where E_f and E_m are the elastic modulus of the fibers (nanotubes) and matrix (polymer) respectively, and V_f is the volume fraction of the fibers. The theoretical elastic modulus for each nanocomposite was calculated using the Halpin–Tsai Equation for random alignment (Equation (4)) and the previously measured/calculated aspect ratios, densities and effective moduli for each type of nanotube (see Table 1). These calculated values have been compared with the actual experimental results in Table 2.

As shown in Table 2, the higher effective modulus of Nanocyl MWNTs (due to their small diameters) leads to a much higher theoretical composite elastic modulus, however the opposite is seen when compared with the experimental results. The higher-than predicted measured elastic modulus of the CSIRO–HDPE

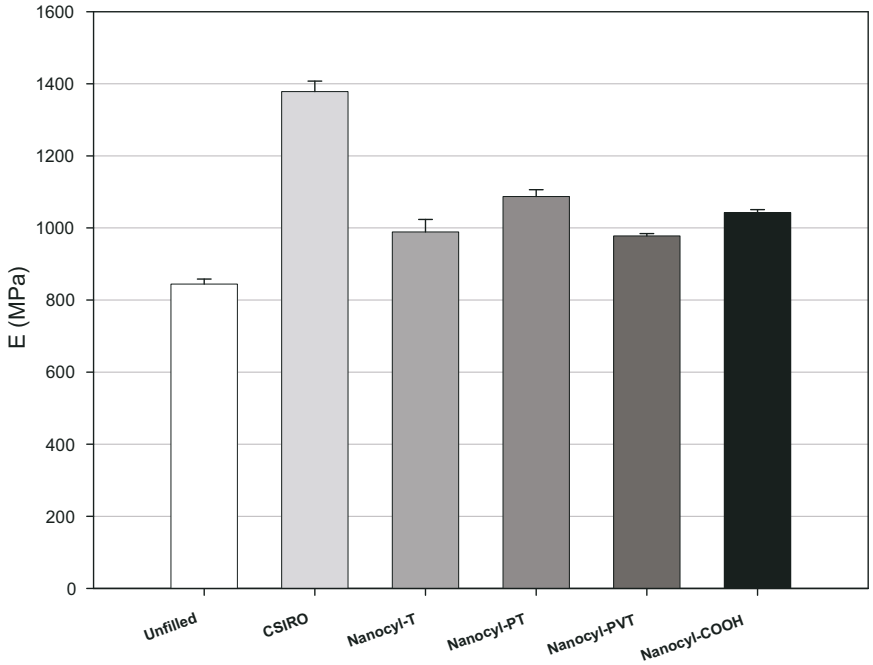

Fig. 6. Effect of the MWNTs on the elastic modulus of HDPE at a loading level of 5 wt%.

composites may be due to the nanotubes aligning during the injection molding process. This is a phenomenon that we have observed in other polymer matrices [9] where SEM analysis of cryo-microtomed sections cut from injection molded tensile specimens shows significantly more nanotubes protruding from sections cut perpendicular to the flow direction than those cut parallel [9]. In comparison, the lower than predicted elastic modulus of the Nanocyl MWNTs is most likely due to the lower dispersion observed in these composites and, for the Nanocyl-PVT and Nanocyl-T MWNTs, due to high concentrations of non-nanotube carbonaceous material and metal oxide particles.

The nanotubes also increase the yield stress of the polymer, with Fig. 7 showing that the CSIRO MWNTs were the most effective, resulting in a 69% increase. When comparing the Nanocyl MWNT–HDPE nanocomposites, the Nanocyl-PT MWNTs provided the largest increases to the yield strength of HDPE (37% increase), followed by the Nanocyl-COOH MWNTs (31% increase). The Nanocyl-T and Nanocyl-PVT MWNTs provided even smaller increases, at 22% and 21% respectively. Interestingly, the more effective nanotubes are those with higher aspect ratios, a finding that correlates to fiber composite theory, where it is found that the average stress carried by a fiber is directly proportional to the fiber's aspect ratio [10].

Characteristic stress–strain curves (Fig. 8) show significant differences in the behavior of the nanocomposites, post yielding. The unfilled tensile specimens show typical HDPE stress–strain behavior, with yielding being followed by the formation of a neck which proceeded to grow along the gauge length, followed by an increase in stress until failure occurred. Stabilization and growth of a neck also occurred in the 5 wt% Nanocyl-T, Nanocyl-PT and Nanocyl-PVT nanocomposites, indicating that polymer chains in the amorphous regions were able to orientate and stretch in the direction of the applied tensile stress, thus overcoming the increase in stress due to the reduced cross-sectional area. However the addition of both the CSIRO and Nanocyl-COOH MWNTs hindered the orientation of the polymer chains to such an extent that failure occurred before this neck could stabilize. In the CSIRO composites this was most likely due to the MWNTs providing a high resistance to polymer chain orientation (as indicated by the high yield stresses in these composites). For the composites in which a neck did stabilize, the stress at which the neck propagated (the draw stress) increased with the addition of MWNTs, with the Nanocyl-PT MWNTs resulting in the largest increase.

The breaking strains of the composites are shown in Fig. 9, with the CSIRO MWNTs providing the greatest reduction in strain at break, down to 33 ± 4% followed closely by the Nanocyl-COOH MWNTs. While the Nanocyl-PT MWNT nanocomposites resulted in a significant reduction in strain at break at this concentration, there was only a small reduction due to the Nanocyl-T and Nanocyl-PVT MWNTs.

Table 2
Comparison between the theoretical elastic modulus of the 5 wt% MWNT–HDPE nanocomposites (as calculated using the Halpin–Tsai Equation for randomly aligned fiber reinforced composites) and the measured elastic modulus from tensile testing.

Nanotubes	E_c (theoretical), MPa	E_c (measured), MPa
CSIRO	1020 ± 30	1380 ± 30
Nanocyl-T	1400 ± 100	990 ± 30
Nanocyl-PT	1600 ± 100	1090 ± 20
Nanocyl-PVT	1800 ± 100	978 ± 6
Nanocyl-COOH	1600 ± 100	1043 ± 8

4. Discussion

The high degree of reinforcement achieved by the CSIRO MWNTS is thought to be largely due to the high level of dispersion achieved by these nanotubes through the melt mixing process. We propose that the aligned nature and low bulk density of these nanotubes would allow an easier path for the polymer to infiltrate between the nanotubes, while their larger diameters would also improve the ability of these materials to be dispersed.

As shown by SEM images in Fig. 1, the CSIRO nanotubes were produced in an aligned forest with a lower bulk density than the Nanocyl MWNTs. The significant spacing between individual

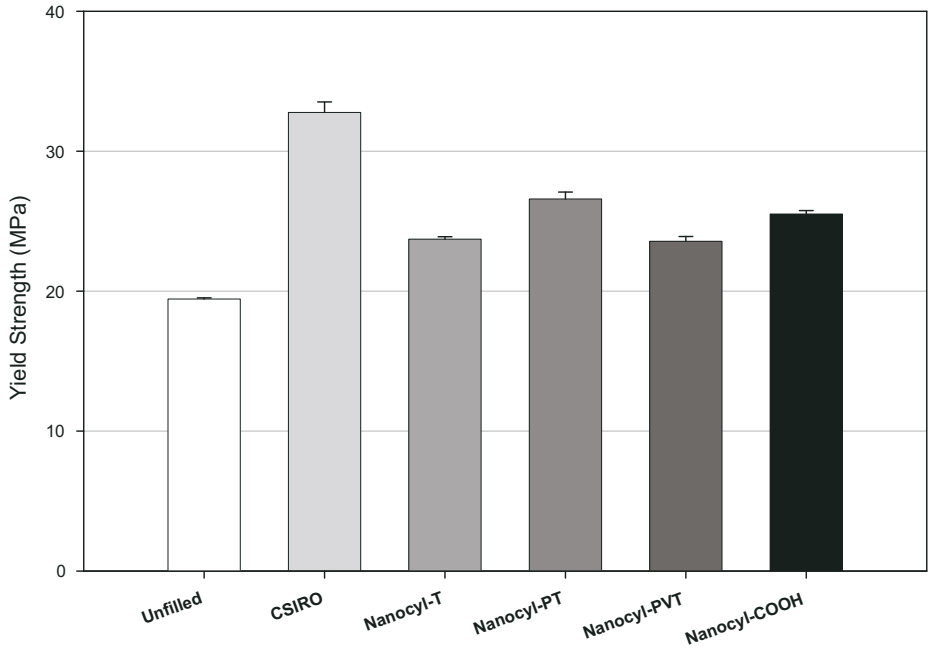

Fig. 7. Effect of the MWNTs on the yield strength of HDPE at a loading level of 5 wt%.

nanotubes combined with the high level of alignment could allow efficient permeation of the polymer thereby encouraging good dispersion and allowing a path through which the polymer could permeate. Although the Nanocyl-T and Nanocyl-PT nanotubes were also received in a relatively aligned form, they had a higher bulk density and this tighter packing would likely provide a higher degree of resistance to the ingress of polymer through the nanotube bundles, resulting in poorer nanotube dispersion. Nanocyl-PVT and Nanocyl-COOH MWNTs however were received in non-aligned states with even higher bulk densities, the Nanocyl-COOH MWNTs occupying less than half the volume per gram compared to the Nanocyl-T MWNTs, and less than a tenth the volume per gram of CSIRO MWNTs, possibly due to the chemical treatment process used to functionalize the nanotubes.

However, the intrinsic ability of the CNTs to self-associate, as opposed to disperse is likely to depend on nanotube diameter, as has been discussed by a few researchers, with many attributing the agglomeration of SWNTs in polymer nanocomposites to their high surface energy [8,11]. In this connection, Neimark [12] showed that fiber curvature is an important factor affecting fiber wettability, a transition from partial wetting to non-wetting occurring as fiber diameter decreases. Modeling studies investigating the thermodynamics of mixing have predicted that dispersion is unfavorable for nanotubes with diameters less than approximately 2 nm. Maiti et al. [13] applied the Flory–Huggins theory to the question of nanotube solubility using mesoscale modeling to calculate the solubility parameter of CNTs as a function of tube diameter and compared this with the solubility parameters of well-known polymers, predicting that nanotubes with diameters greater than approximately 1.8 nm are soluble in polyethylene. Another study by Nyden and Stoliarov [14] calculated the energy of mixing of carbon nanotubes into polystyrene, taking into account the energy needed to exfoliate bundles of nanotubes. They found that at absolute zero the energy of mixing became exothermic when the nanotube diameters were greater than 2.2 nm, this critical diameter decreasing slightly as temperature is increased. They suggested that the thermodynamics of mixing becomes more favorable with increasing diameter because the attraction between nanotubes per unit surface area decreases, while the attraction between CNTs and polymer is approximately constant for nanotubes with diameters greater than 1 nm.

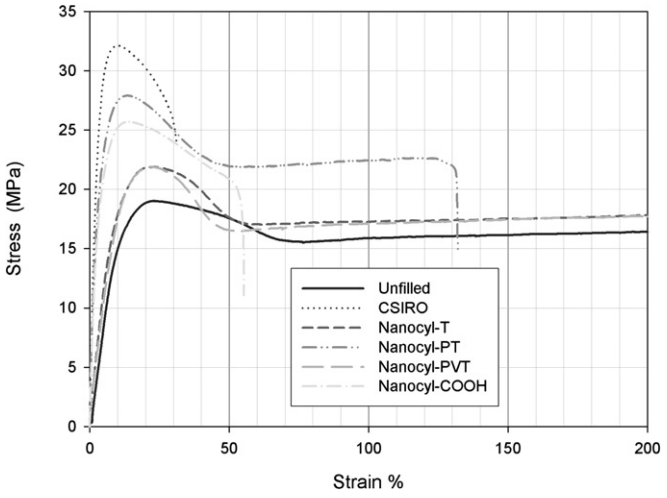

Fig. 8. Stress–strain curves for the 5 wt% MWNT–HDPE nanocomposite.

While the thinnest nanotubes studied in this work have diameters greater than 2 nm (and therefore dispersion is likely to be somewhat thermodynamically favorable), the attraction between nanotubes (per unit surface area) still decreases with increasing nanotube diameter [14]. Therefore, the energy required to separate bundles of the thinnest Nanocyl MWNTs would be significantly higher than for the larger CSIRO MWNTs.

In addition, it is also likely that thinner nanotubes become increasingly more difficult to wet and disperse due to the distance between dispersed nanotubes in a matrix approaching the size of polymer molecules [15,16]. Shaffer and Kinloch [15] calculated that if one could produce a well dispersed SWNT composite at a loading of 1 vol%, then every polymer molecule would be within 5 nm of a nanotube. Since this separation is of a similar order to the radius of gyration of typical polymers, they predicted that wetting would become difficult due to constraint from the matrix.

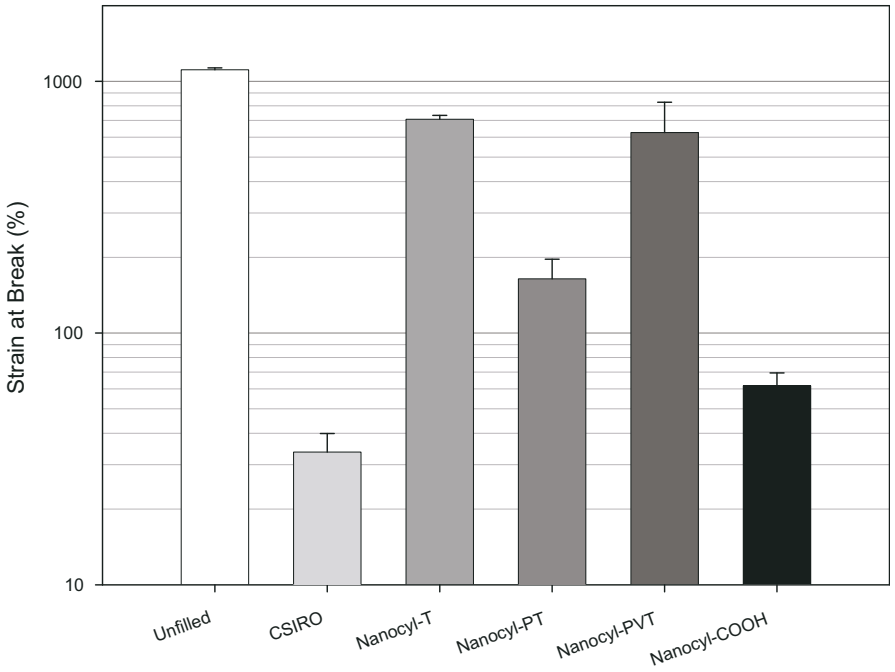

Fig. 9. Effect of the various MWNTs on the breaking strain of HDPE at a loading level of 5 wt%.

Using this concept, we have calculated the maximum distance that a polymer molecule will be from a nanotube in our composites if full wetting and good dispersion of the nanotubes is achieved. To do this we used a model where the nanotubes were aligned and evenly dispersed in an array based on the basal plane of the hexagonal close packed (HCP) structure, resulting in the maximum distance between a polymer chain and a CSIRO nanotube of 150 nm (at a 5 wt% loading) compared with 18 nm for the Nanocyl-PVT MWNTs and 30 nm for the Nanocyl-T MWNTs. The radius of gyration (R_g) of our HDPE390 (with a molecular weight of 59 900) should be approximately 10.7 nm [17]. Therefore if good wetting and dispersion was achieved for the 5 wt% Nanocyl–HDPE composites, every polymer chain would be within $1.6R_g$–$3R_g$ of an interface. In this case all the polymer molecules could be classed as being in the interfacial region (which nominally extends into the bulk one to four times the radius of gyration of the matrix [18]), a region where the mobility of the polymer molecules is frequently reduced, suggesting that dispersion may be more difficult for the thinner Nanocyl MWNTs compared to the larger diameter CSIRO MWNTs.

5. Conclusions

Although nanotubes of thinner diameter theoretically provide superior reinforcement to polymers, in this study the reverse was found, the highest degree of reinforcement (in terms of increase in elastic modulus and yield strength) being provided by larger diameter nanotubes.

The higher degree of reinforcement is thought to be due to the better quality of dispersion achieved by these nanotubes in the HDPE under melt mixing than their thinner counterparts.

We propose that the higher degree of dispersion achieved by the larger diameter, CSIRO MWNTs is related to a combination of factors. Firstly, although dispersion of the thin nanotubes studied in this work is predicted to be thermodynamically favorable, the attraction between nanotubes decreases with increasing nanotube diameter, resulting in the driving force towards dispersion being higher for larger diameter nanotubes. Secondly, as nanotubes become thinner it is thought they become increasingly more difficult to wet and disperse due to the distance between nanotubes approaching the size of polymer molecules, our calculations showing that every polymer chain is within $1.6R_g$–$3R_g$ of an interface for the 5 wt% Nanocyl MWNT–HDPE composite, resulting in the majority of the polymer being within the interfacial region where polymer mobility may be reduced, while for the CSIRO MWNTs, this distance is increased to $14R_g$. Finally, the larger diameter CSIRO nanotubes were received in an aligned and well separated form with significantly lower bulk density than the thinner Nanocyl MWNTs. The relatively large spacing between nanotubes would have allowed an easy path for the thermoplastic melt to penetrate the bundles and wet the nanotubes during melt mixing, while the alignment would likely have reduced nanotube entanglement, encouraging exfoliation.

In this work purification of the Nanocyl MWNTs was found to increase the reinforcing effectiveness of the MWNTs, while functionalization had a negative effect. This reduction in reinforcement is most likely related to these nanotubes being in a more densely tangled form that was more difficult to disperse in the polymer melt in addition to interactions between functional groups on the surfaces of these nanotubes likely inhibiting their dispersion in the non-polar HDPE.

The aspect ratio of the nanotubes was also found to be important, with yield strength of composites being higher for those composites with nanotubes having larger aspect ratios.

Acknowledgements

The authors wish to thank Dr Ravi Krishnamoorthy from NanoVic, for providing the Nanocyl MWNTs as well as Chi Huynh and Stephen Hawkins from CSIRO Materials Science and Engineering, Australia for producing and supplying the CSIRO MWNTs.

References

[1] Thostenson ET, Chou TW. Journal of Physics D: Applied Physics 2003;36(5): 573–82.

[2] Gojny FH, Wichmann MHG, Fiedler B, Schulte K. Composites Science and Technology 2005;65(15–16):2300–13.
[3] Cadek M, Coleman JN, Ryan KP, Nicolosi V, Bister G, Fonseca A, et al. Nano Letters 2004;4(2):353–6.
[4] Potschke P, Fischer D, Simon F, Haußler L, Magrez A, Forró L. Macromolecular Symposia 2007;254(1):392–9.
[5] Andrews R, Jacques D, Rao AM, Derbyshire F, Qian D, Fan X. Chemical Physics Letters 1999;303(5–6):467–74.
[6] Yakobson BI, Smalley RE. American Scientist 1997;85(4):324–37.
[7] Lu JP. Physical Review Letters 1997;79(7):1297–300.
[8] Coleman JN, Khan U, Blau WJ, Gun'ko YK. Carbon 2006;44(9):1624–52.
[9] Morcom M. Carbon nanotube polymer composites. Materials Engineering, PhD. Clayton: Monash; 2008. pp. 318.
[10] Bowyer W, Bader M. Journal of Materials Science 1972;7(11):1315–21.
[11] Zhang N, Xie J, Varadan VK. Smart Materials and Structures 2002;11(6):962–5.
[12] Neimark AV. Journal of Adhesion Science and Technology 1999;13(10):1137–54.
[13] Maiti A, Wescott J, Kung P. Molecular Simulations 2005;31(2–3):143–9.
[14] Nyden MR, Stoliarov SI. Polymer 2008;49(2):635–41.
[15] Shaffer M, Kinloch IA. Composites Science and Technology 2004;64(15):2281–2.
[16] Coleman JN, Khan U, Gun'ko YK. Advanced Materials 2006;18(6):689–706.
[17] Lieser G, Fischer EW, Ibel K. Journal of Polymer Science: Polymer Letters Edition 1975;13(1):39–43.
[18] Vaia RA, Wagner HD. Materials Today 2004;7(11):32–7.